Electronic supplementary information (ESI†)

Synergistic Defect Engineering and Microstructure Tuning in Lithium Tantalate for High-contrast Mechanoluminescence of Bi^{3+}: Toward Application for Optical Information Display

Rui Hu[a,b,c], Ying Zhang[d], Yan Zhao[a], Xusheng Wang[a*], Guorong Li[b*] and Mingxue Deng[b,c]

a. *Key Laboratory of Advanced Civil Engineering Materials of the Ministry of Education, Functional Materials Research Laboratory, School of Materials Science and Engineering, Tongji University, Shanghai 201804, China*

b. *Key Laboratory of Inorganic Functional Material and Device, Shanghai Institute of Ceramics, Chinese Academy of Sciences, Shanghai 200080, China*

c. *University of Chinese Academy of Sciences, Beijing 100049, China*

d. *Shanghai Institute of Microsystem and Information Technology, Chinese Academy of Sciences, Shanghai 200050, China*

[*]*Corresponding authors:*

E-mail: xs-wang@tongji.edu.cn (X. W.).

E-mail: grli@sunm.shcnc.ac.cn (G. L.).

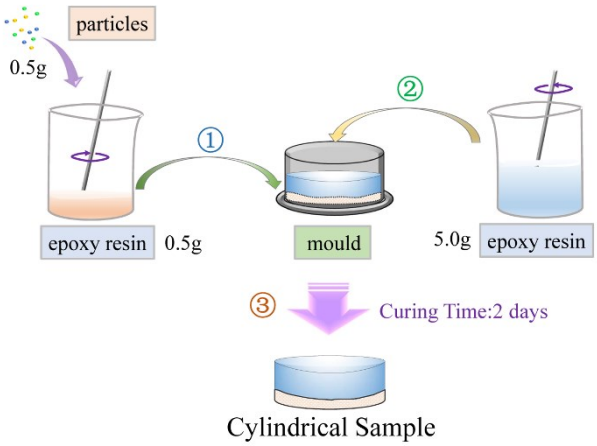

Fig. S1 Preparation process routing of cylindrical bulk.

The as-prepared phosphor particles (0.5 g) were screened firstly then added into 0.5 g as-prepared epoxy resin. Next, the mixture was stirred adequately and transferred into a cylindrical mould. Second, another 5.0 g epoxy resin solution was poured into the mould. Third, the semi-finished product was solidified at room temperature for 2 days. When solidified completely, the cylindrical sample was lifted out from mould and deburred carefully.

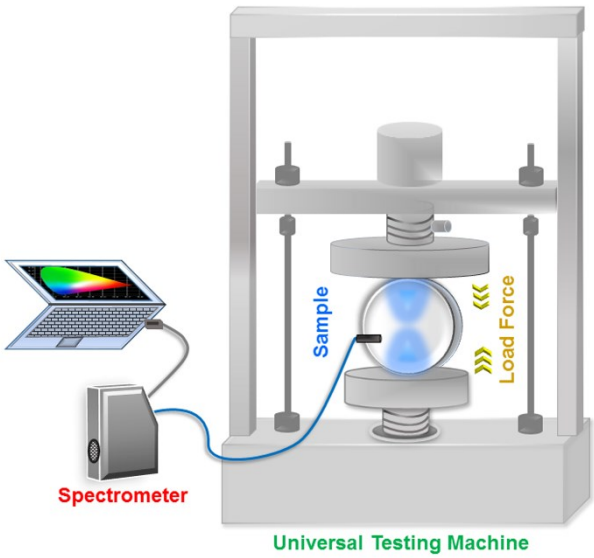

Fig. S2 The graphic expression of testing processes for ML performance. Before the ML measurement, samples were pre-irradiated upon 254 nm UV-light for 5 min, and decayed in the dark for 3 min in order to removing afterglow interference.

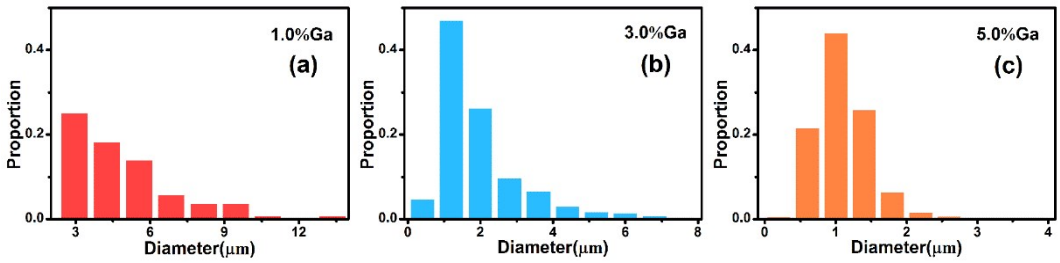

Fig. S3 The bar charts of the size distribution for $LiTaO_3$:1.0%Bi^{3+}/$x$$Ga^{3+}$ samples (x = 1.0%, 3.0% and 5.0%).

As shown in Fig. S3, the grain size of particles decreased continually with Ga^{3+} concentration increasing. The mean grain size of samples is 3.91 μm (1.0%Ga^{3+}), 1.92 μm (3.0%Ga^{3+}) and 1.08 μm (5.0%Ga^{3+}) respectively. Phosphor particle distribution suggests that $LiTaO_3$:1.0%Bi^{3+}/1.0%Ga^{3+} particles are mainly large size, and their distribution is uneven (ranging from 2.0 to 10.0 μm). With Ga^{3+} content increasing, the mean grain size decreased obviously, meanwhile the uniformity of particles was also improved. Especially, the grain size distribution of $LiTaO_3$:1.0%Bi^{3+}/5.0%Ga^{3+} phosphor shows marked improvement which centered on 0.5-1.5 μm.

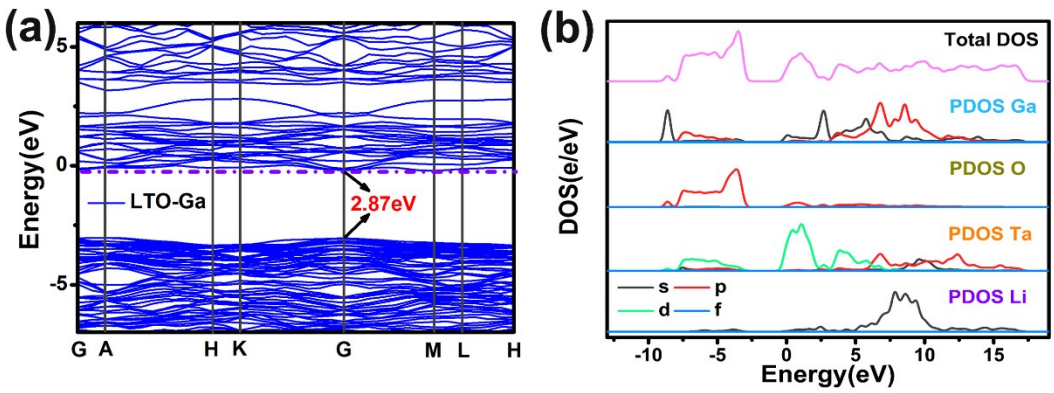

Fig. S4 (a) The electronic band structure of Ga^{3+} doped $LiTaO_3$ (LTO) along the path of high symmetrical points in the reciprocal Brillouin zone. (b) Partial density of states for $LiTaO_3$:Ga.

On base of 4×4×2 super cell model, the calculation of electronic structure was operated using the Perdew-Burke-Ernzerhof exchange-correlation function within generalized gradient approximation (GGA-PBE).

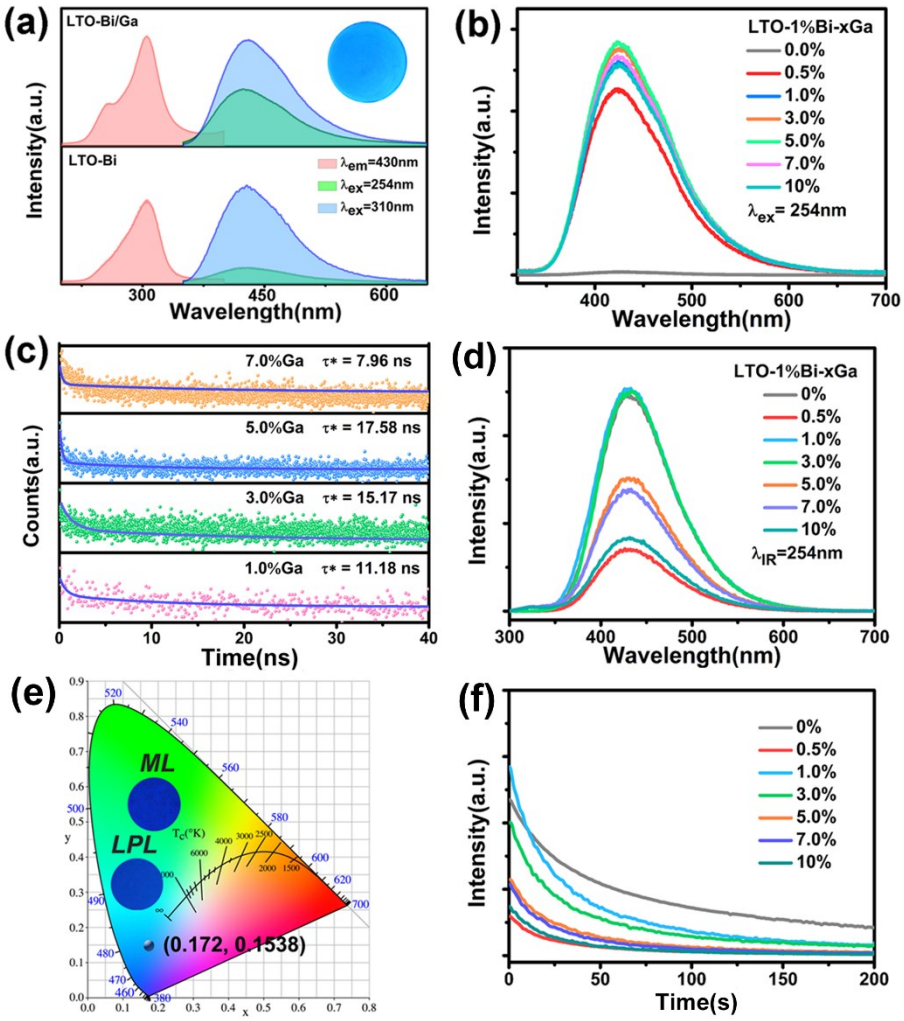

Fig. S5 (a) PLE and PL spectra of $LiTaO_3$:1.0%Bi^{3+} (LTO-Bi) and $LiTaO_3$:1.0%Bi^{3+}/1.0%Ga^{3+} (LTO-Bi/Ga), inset is the photograph of LTO-Bi/Ga phosphor under 254 nm excitation. (b) PL spectra of $LiTaO_3$:1.0%Bi^{3+}/x%Ga^{3+} (x = 0.0-10.0) under 254 nm excitation. (c) Fluorescence decay curves of typical $LiTaO_3$: Bi/Ga samples (λ_{em} = 430 nm, and λ_{ex} = 250 nm). (d) LPL spectra of $LiTaO_3$:1.0%Bi^{3+}/x%Ga^{3+} (x = 0.0-10.0) after 254 nm irradiation. (e) Phosphorescence chromaticity coordinate of $LiTaO_3$:1.0%Bi^{3+}/1.0%Ga^{3+}, insets are its LPL and ML emission photographs. (f) LPL lifetime curves of $LiTaO_3$:1.0%Bi^{3+}/x%Ga^{3+} (x = 0.0-10.0).

Bi^{3+} ions were the single PL emitting center which showed indigo blue color, and the PL spectra exhibited no obvious transformation in peak shape or quantity with Ga^{3+} concentration increasing, even Ga^{3+} dopant could improve the emission intensity of Bi^{3+} activators observably (presented in Fig. S5a-b). Under 254 nm excitation, all samples had a broad emission band peaked at ~430 nm, which displayed indigo blue light to naked eye.

Interestingly, even a low concentration of Ga^{3+} co-dopants could significantly increase the PL emission intensity of Bi^{3+} activators in $LiTaO_3$ matrix (Fig. S5b). In addition, the intensity of PL emission reached extremum value when the concentration of Bi^{3+} dopants increased to 5.0 mol%. The decay curves as well as the relative exponential fitting curves of $LiTaO_3$:1.0%Bi^{3+}/*x*%Ga^{3+} samples monitored at 430 nm are presented in Fig. S5c. These curves obey the second-order exponential and could be fitted with:[1]

$$I(t) = I_0 + A_1 \exp(-t/\tau_1) + A_2\, exp(-t/\tau_2) \quad (1)$$

where *t* represents the time, *I*(t) is the corresponding PL intensity, A_1 and A_2 denote the constants of fitted function, τ_1 and τ_2 are the rapid and slow decay times for exponential components. With these parameters, the average PL emission decay time τ^* can be obtained with the formula as:[2]

$$\tau * = (A_1{\tau_1}^2 + A_2{\tau_2}^2)/(A_1\tau_1 + A_2\tau_2) \quad (2)$$

The calculated results of τ^* are 11.18, 15.17, 17.58 and 7.96 ns, corresponding to *x* of 1.0%, 3.0%, 5.0% and 7.0%, respectively. The fitted average decay time (τ^*) of Bi^{3+} PL emission increased with Ga^{3+} content enhancing from 1.0% to 5.0%, which is longer than the lifetime of single-doped $LiTaO_3$:Bi sample (~3 ns).[3] The fluorescence decay curves proves the energy transfer process in $LiTaO_3$:Bi/Ga phosphors. With the increasing of Ga^{3+} ions concentration, the distance between activator ions increases, but the efficiency of energy transfer from Ga^{3+} to Bi^{3+} ions is improved concurrently. Namely, the average decay time

would be extended. Usually, the decay time of $^3P_0 \rightarrow {}^1S_0$ transition is commonly several hundred microseconds since this transition is always forbidden. Nevertheless, the $^3P_1 \rightarrow {}^1S_0$ transition is Laporte-allowed, the corresponding PL emission at room temperature has shorter decay time ranging from 10^{-6} to 10^{-8} s.[4] Thus, the PL emission of Bi^{3+} in $LiTaO_3$ crystal mainly originates from $^3P_1 \rightarrow {}^1S_0$ transition. This result indicates that Ga^{3+} dopant gives rise to energy transfer from valance band and Ga^{3+} ions to Bi^{3+} ions, thus the decay time of Bi^{3+} is improved, resulting in intensifying PL emission. As shown in Fig. S5d, long-persistent luminescence spectra similarly owned single broad emission band peaked at 430 nm, the emission intensity had negative correlation with Ga^{3+} concentration, which decreased the initial LPL intensity and the afterglow lifetime of samples obviously. As shown in Fig. S5e, the chromaticity coordinate of $LiTaO_3$:1.0%Bi^{3+}/1.0%Ga^{3+} is (0.172, 0.1538) indicating that the ML emission of $LiTaO_3$:1.0%Bi^{3+}/1.0%Ga^{3+} is similar to its LPL emission. $LiTaO_3$:Bi phosphor obtained durable afterglow longer than 6 min after stopping UV irradiation, meanwhile the afterglow of $LiTaO_3$:Bi/Ga almost disappeared in 3 min (Fig. S5f). This speciality of fast attenuation is in favor of the development of no-interference reading or display materials for optical information.[5]

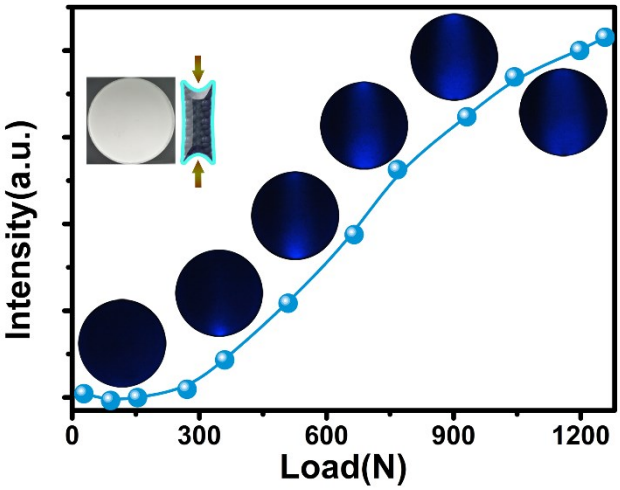

Fig. S6 Linear ML intensity response of cylinder sample (x = 5.0%) as a function of compressive load, the insets are a sequence of transient ML photographs recorded at different load.

Then we used a $LiTaO_3$:1.0%Bi^{3+}/5.0%Ga^{3+} cylinder which obtained optimal ML intensity to evaluate the response and duplication performances of this composite material within a wide compressive load range (0-1200 N). Under successive compression load, the ML emission intensity increased linearly with the compressive force from ~150 N. As the load increased, the ML attributed to Bi^{3+} dopants presented a brighter and broader spindle-shaped distribution (upper right insets of Fig. S6) that accurately reflected the stress distribution, indicating the ML pattern of dynamic stress visualization.[6]

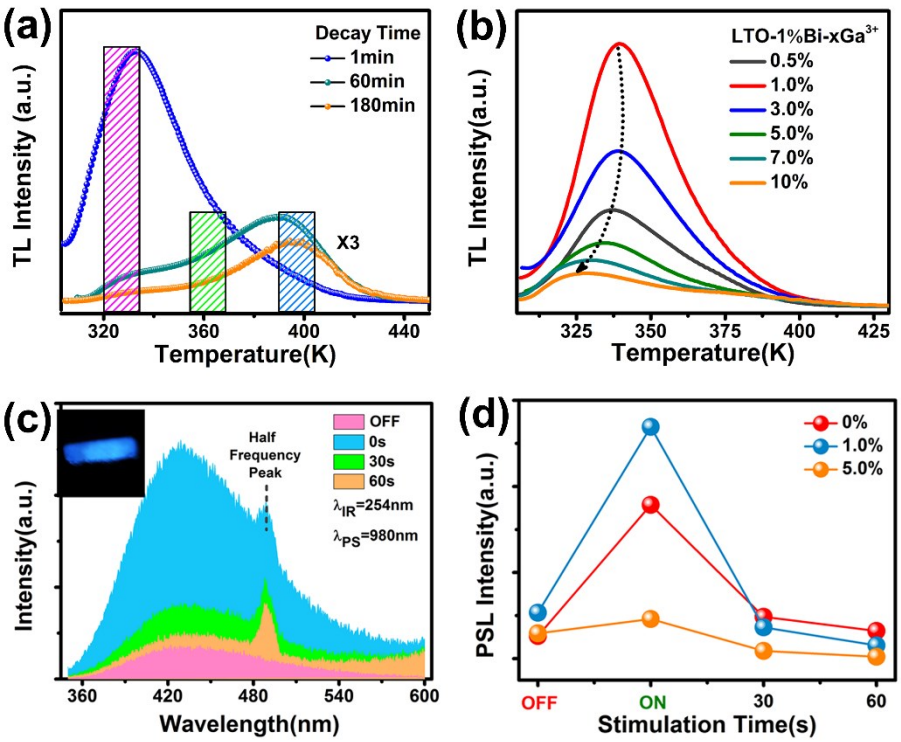

Fig. S7 (a) TL curves of $LiTaO_3$:1.0%Bi^{3+}/5.0%Ga^{3+} placed in the dark for different periods of time. (b) TL curves of $LiTaO_3$:1.0%Bi^{3+}/x%Ga^{3+} (x = 0.5-10.0) phosphors. (c) PSL emission spectra of $LiTaO_3$:1.0%Bi^{3+}/1.0%Ga^{3+} taken under varying 980 nm laser stimulation time (off, 0, 30 and 60 s), the inset shows corresponding photograph of PSL emission. (d) Change of PSL intensity for $LiTaO_3$:Bi and typical $LiTaO_3$:Bi/Ga samples with 980 nm laser stimulation time.

The LPL emission spectrum of $LiTaO_3$:Bi/Ga phosphor is similar to that of $LiTaO_3$:Bi phosphor, which has broad emission band peaked at 430 nm. The initial intensity of afterglow for $LiTaO_3$:Bi/Ga is stronger than that of $LiTaO_3$:Bi phosphor after identical pre-irradiation, but their afterglow decay rates have different features. According to the afterglow decay curves, Ga^{3+} co-dopants can accelerate the attenuation of afterglow, which is beneficial to no-interference ML performance. The TL curves demonstrate that Ga^{3+} ions increase the proportion of shallow traps in trap distribution and reduce the content of deep traps, resulting in the reduction of afterglow lifetime.

After decaying in the dark for 180 min, charge carriers trapped in shallow traps were

almost completely emptied, but, meanwhile, there were still enough charge carriers in middle and deep traps for maintaining ML emitting under mechanical stimuli (Fig. S7a). As shown in Figure S7b, low Ga^{3+} concentration (0-1.0%) will improve the content of middle traps, because Ga^{3+} ions can occupy massive lithium vacancies and generate gallium ion defects. When the Ga^{3+} concentration increases sequentially, they will enter into interstitial lattice sites and form defect clusters that can promote the recombination of excited electrons and holes. Namely, the signals representing the content of defect traps in TL curves decrease continually. Typically, photostimulated luminescence can assist in characterizing the feature of defect traps, and the $LiTaO_3$:Bi/Ga samples can also exhibit typical PSL phenomenon under 980 nm laser irradiation. The PSL light of $LiTaO_3$:Bi/Ga phosphor showed indigo blue color related to Bi^{3+} activators and would weaken as the exposure time prolonged (Fig. S7c). With the concentration of Ga^{3+} increasing, the initial PSL intensity reduced suggesting that the content of defect traps decreased due to the introduction of defect clusters (Fig. S7d). Particularly, $LiTaO_3$:Bi sample could sustain more durable PSL emission under 980 nm laser irradiation, indicating that there were more deep traps in Bi^{3+} single-doped $LiTaO_3$ crystal.

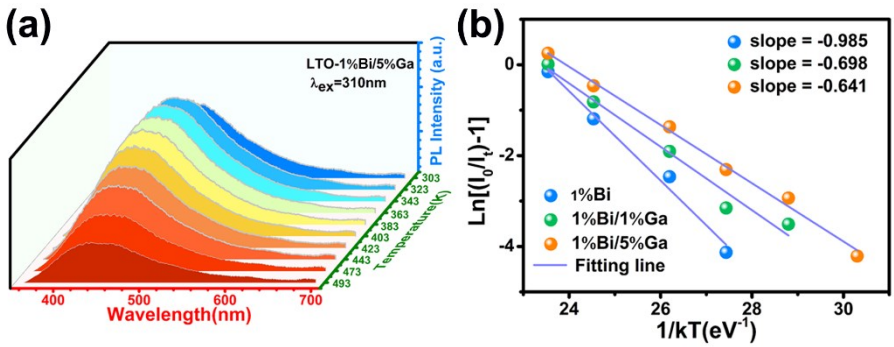

Fig. S8 (a) Temperature-dependent PL spectra of $LiTaO_3$:1.0%Bi^{3+}/5.0%Ga^{3+} sample. (b) Arrhenius fitting of the PL intensity in $LiTaO_3$:1.0%Bi^{3+}, $LiTaO_3$:1.0%Bi^{3+}/1.0%Ga^{3+} and $LiTaO_3$:1.0%Bi^{3+}/5.0%Ga^{3+} samples.

Fig. S8a represents the temperature-dependent PL spectra of $LiTaO_3$:1.0%Bi^{3+}/5.0%Ga^{3+} under 310 nm excitation (ranging from 303 K to 493 K in a step of 20 K). According to the Arrhenius equation,[1] the activation energy (ΔE) for thermal quenching was calculated via the slope of line in Fig. S8b. The calculated values were 0.985, 0.698 and 0.641 eV for 0.0%, 1.0% and 5.0% Ga^{3+}-doped sample respectively. The reduction of activation energy further affirms the enhancement of microstructure distortion.

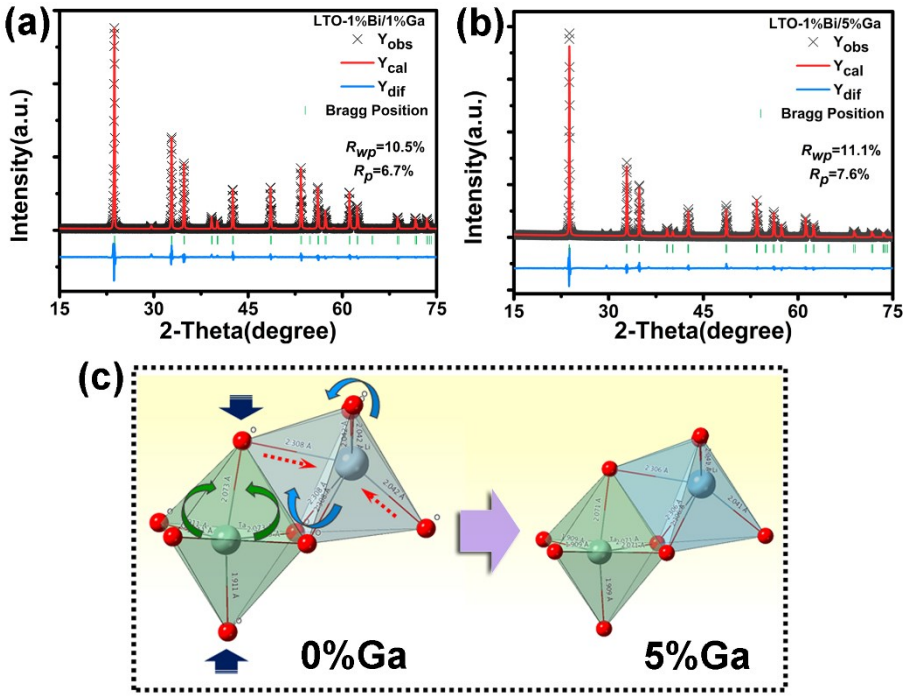

Fig. S9 (a-b) XRD Rietveld refinement of typical $LiTaO_3$:Bi/Ga samples. (c) Schematic illustration of octahedral distortion ([LiO_6] and [TaO_6] octahedron) induced by Ga^{3+} ions.

To further confirm the microstructure distortion in matrix, we investigated the detailed crystal structure of $LiTaO_3$:Bi and $LiTaO_3$:Bi/Ga via Rietveld refinement process. The final refinement results converge to R_{wp} = 10.5%/ R_p = 6.7% ($LiTaO_3$:1.0%Bi^{3+}/1.0%Ga^{3+}) and R_{wp} = 11.1%/ R_p = 6.7% ($LiTaO_3$:1.0%Bi^{3+}/5.0%Ga^{3+}), respectively.

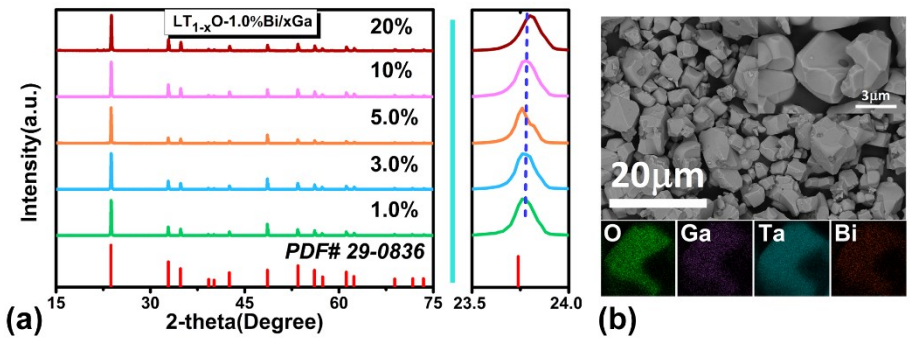

Fig. S10 Crystal structure and morphology characterization of typical $LiTa_{1-x}O_3$:Bi/Ga samples ($LT_{1-x}O$). (a) XRD patterns of $LiTa_{1-x}O_3$:1.0%Bi^{3+}/$x$$Ga^{3+}$ (x = 1.0-20.0%) and correlative magnified 2-theta region of 23.5-24.0°. (b) SEM image of $LiTa_{0.95}O_3$:1.0%Bi^{3+}/5.0%Ga^{3+} phosphor, the insets show the enlarged view of phosphor particles, and EDX elemental distribution maps of its particles (bottom).

All XRD patterns of synthesized samples (Fig. S10a) were similarly in agreement with standard reference data for JCPDS no. 29-0836, indicating that the tantalum deficiency in synthesis process introduced no other secondary phases. Ga^{3+} ions caused slight shrink of lattice because Ga^{3+} ions (r = 0.62 Å, CN = 6) preferentially occupied Ta^{5+} (r = 0.64 Å, CN = 6) vacancies, but would not induce element enrichment or segregation in particles (right of Fig. S10a, Fig. S10b).[7] These results demonstrate the feasibility of tantalum-ion shortfall strategy in material preparation.

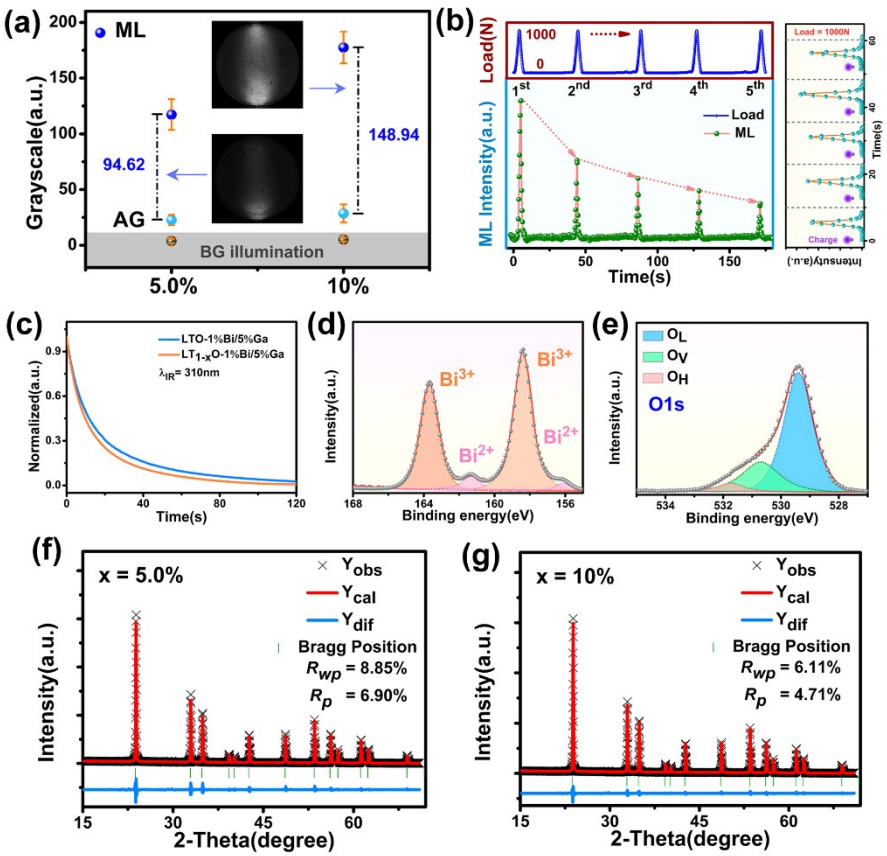

Fig. S11 (a) Gray value on different area of $LiTa_{0.95}O_3$:1.0%Bi^{3+}/5.0%$Ga^{3+}$and $LiTa_{0.90}O_3$:1.0%Bi^{3+}/10.0%Ga^{3+} cylinder samples, insets are grayscale images of ML emitting. (b) ML intensity decay curve under consecutive load cycles (left) and ML recovery behavior after UV irradiation (right). (c) LPL lifetime curves of $LiTaO_3$:1.0%Bi^{3+}/5.0%Ga^{3+} and $LiTa_{0.95}O_3$:1.0%Bi^{3+}/5.0%Ga^{3+} after 310 nm irradiation. (d)-(e) XPS core level spectra of Bi 4f, O 1s for $LiTa_{0.95}O_3$:1.0%Bi^{3+}/5.0%Ga^{3+} phosphor. (f)-(g) XRD Rietveld refinement of typical $LiTa_{1-x}O_3$:1.0%Bi^{3+}/$x$$Ga^{3+}$ samples.

The overall ML intensity still stayed in about 20% that of the initial peak value after five cycles (left of Fig. S11b), moreover, the ML emission similarly showed a typical recoverable performance after multiple cycles of Charging-Compressing process (as shown in the right of Fig. 11b). The structure refinement of $LiTa_{0.95}O_3$:1.0%Bi^{3+}/5.0%Ga^{3+} and $LiTa_{0.90}O_3$:1.0%Bi^{3+}/10.0%Ga^{3+} are presented in Fig. S11f-g. The final obtained residual R-factors of R_{wp} and R_p were determined to be 8.85% and 6.90% for $LT_{0.95}O$:1.0%Bi^{3+}/5.0%Ga^{3+}, 6.11% and 4.71% for $LT_{0.90}O$:1.0%Bi^{3+}/10.0%Ga^{3+}. Based on

the Rietveld refinement data, the volume of [LiO_6] octahedron in $LiTa_{1-x}O_3$:Bi/Ga was improved, which was opposite to that of [TaO_6] octahedron. The σ^2 of [LiO_6] in tantalum-deficiency sample also increased to113.71 by Ga^{3+} co-dopants, but as for [TaO_6] octahedron, the value decreased to 53.17. The $<\lambda>$ of [LiO_6] octahedron increased slightly as the Ga^{3+} ions were doped, while the relevant parameter of [TaO_6] octahedron became smaller. The result confirmed that Ta^{5+} vacancies were mainly filled with Ga^{3+} ions, then the newly generated defects strengthened microstructure distortion due to valence and radii mismatch between Ga^{3+} ions and Li^{+}/Ta^{5+} ions.

Table S1 Change of octahedral angle variance (σ^2), mean quadratic elongation (<λ>) and octahedral volume (V) for [LiO_6] and [TaO_6] octahedron with Ga^{3+} ion concentration in typical $LiTa_{1-x}O_3$:Bi/Ga samples.

Sample	[LiO_6] Octahedron			[TaO_6] Octahedron		
	σ^2	<λ>	V(Å^3)	σ^2	<λ>	V(Å^3)
1%Bi/5%Ga	13.28	1.34	10.569	285.04	1.44	11.518
1%Bi/10%Ga	113.71	1.35	11.773	53.17	1.34	10.437

Reference

[1] K. Li, H. Lian, M. Shang, J. Lin, *Dalton T.*, 2015, **44**, 20542.

[2] L. Jiang, R. Pang, D. Li, W. Sun, Y. Jia, H. Li, J. Fu, C. Li, S. Zhang, *Dalton T.*, 2015, **44**, 17241.

[3] R. Hu, Y. Zhang, Y. Zhao, X. S. Wang, G. R. Li, C. Y. Wang, *Chem. Eng. J.*, 2020, **392**, 124807.

[4] F. W. Kang, Y. Zhang, L. Wondraczek, J. Zhu, X. Yang, M. Y. Peng, *J. Mater. Chem. C*, 2014, **2**, 9850.

[5] Y. X. Zhuang, L. Wang, Y. Lv, T. L. Zhou, R. J. Xie, *Adv. Funct. Mater.* 2018, **28**, 1705769.

[6] J. C. G. Bünzli, K. L. Wong, *J. Rare Earth.*, 2018, **36**, 1.

[7] R. D. Shannon, *Acta Cryst.* 1976, **A32**, 751